The Active CryoCubeSat Project: System Modeling and Control Design

Bruno Mattos, Lucas Anderson, Randy Christensen, Charles Swenson
Center for Space Engineering
Utah State University
4130 Old Main Hill, Logan, Utah 84321
mattos@aggiemail.usu.edu

ABSTRACT

Utah State University together with the NASA Jet Propulsion Laboratory have been developing new cooling technology for high power CubeSats. This effort has been funded by the NASA Space Technology Mission Directorate in an effort to enable CubeSats with extraordinary thermal control needs for subsystems such as computing, telemetry, or cryogenics and where passive techniques are insufficient. The approach is to use a pumped fluid loop to remove heat from an internal heat exchanger and transport it to an external radiator on the CubeSat. Recently, Utah State has thermal vacuum-tested prototype systems collecting significant amounts of data on the thermodynamics of pumped fluid loops for small spacecraft. This paper presents the model-based thermal feedback and control system design for Utah State's Active CryoCubeSat prototype. This system is based on a single-phase, two-stage mechanically pumped fluid system, designed to support 6U CubeSat platforms and above. The system modeling was conducted using two different approaches. First, a physical model was derived from the first principle equations, then a system identification was conducted using data collected from the thermal vacuum chamber test of the ACCS system. This paper presents the results and comparison of both models, as well as their limitations in describing the physical behavior of the system. Based on those models, a control system was designed and tuned to achieve a series of thermal requirements for the thermal control of a small cryocooler supporting an infra-red detector at 70 to 120K.

INTRODUCTION

The Active CryoCubeSat (ACCS) was developed to test and prove the concepts of a combined miniature mechanically pumped fluid loop (MPFL) with a micro cryocooler for the thermal control of IR instruments on Small Satellites. This project was funded by the NASA Small Spacecraft Technology Program (SSTP) and conducted by the Center for Space Engineering (CSE) at Utah State University (USU) in partnership with the Jet Propulsion Laboratory (JPL).[1]

Following the successful d ACCS project, the Active Thermal Architecture (ATA) project was initiated with a focus on advancing the application of the ACCS miniature pumped fluid loop technology in 6U CubeSats.[2] Figure 1 shows the 1U CAD-based design of the ATA test article as well as the prototyped placed within a conceptual 6U structure. The ACCS test article consists of a single-axis movable radiator, a micro cryocooler mounted on the heat exchanger of the pumped fluid loop, and a mockup instrument focal plane thermally connected to the cryocooler with vibration isolation.

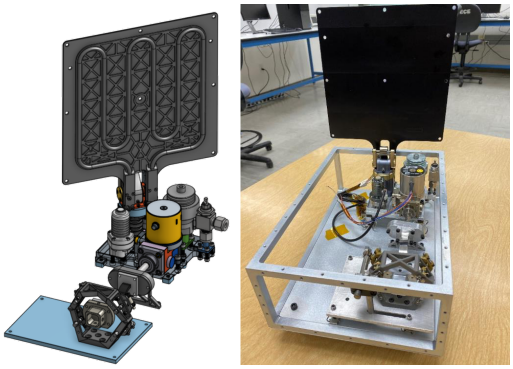

Figure 1: ATA CAD model (right) and the completed test article integrated into a 6U CubeSat prototype structure.

The ACCS development included extensive thermal vacuum chamber testing of a highly instrumented miniature pumped fluid loop with a cryocooler as the heat load. Based on the ACCS design and test data a series of analytical and numerical-based design tools were created, allowing for a rapid and design of the flight like ATA system. This paper presents the system modeling performed for the ACCS subsystem, which will serve as a reference model for the design of the ATA's feedback control system, as well as for the design and optimization of the ATA for different CubeSats sizes and thermal requirements.

The ACCS modeling was performed by two different approaches. First, a physical model was generated by the thermal characterization of the main ACCS components and their physical interfaces. The details and assumptions of this model are presented in the section ACCS PHYSICAL MODELLING. Second, the system identification was performed based on the analysis of thermal vacuum (TVAC) test data. The data collection and analysis used to derive the linear models for the system identification are presented in the section ACCS SYSTEM IDENTIFICATION.

The SIMULATION RESULTS section presents a comparison between the physical model prediction against the TVAC measured data and linear models. A discussion about the limitations of the linear model to characterize the correct pump behavior in the desired range of operation is also presented.

Finally, the CONTROL DESIGN section presents a closed-loop feedback control system designed and tuned based on the ACCS physical model. The PID controller adjusts the pump power to stabilize the Heat Exchanger temperature at the desired value, while the cryocooler maintains the cold tip at some cryogenic temperature.

Concept of operation

Both the ACCS and the subsequent ATA systems are based on the same principle: the heat flux at the heat exchanger is transferred to the thermal fluid, transported to the radiator, and rejected to cold space.

For the use case of a micro cryocooler mounted on the heat exchanger (HX), the system operational concept can be seen as two stages, with a single-phase MPFL serving as the first stage and the cryocooler as the second stage, as illustrated in Figure 2.[3]

Figure 2: Two-stages active thermal architecture

Due to its appropriate size for CubeSats applications, efficiency, and expanded lifetime, the cryocooler selected and tested in the ACCS and also integrated into the ATA subsystem was the Ricor K508N, shown in Figure 3.

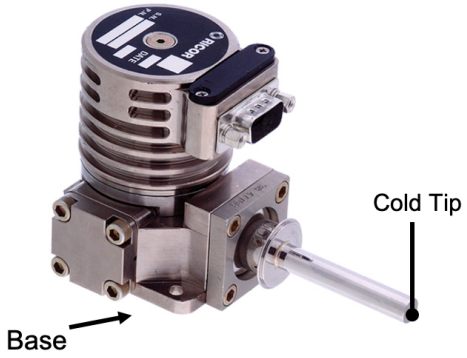

Figure 3: Ricor K508N Cryocooler[4]

For reference, the Ricor K508N can reject up to 650mW from the Cold Tip while keeping the Cold Tip temperature at 80K, and up to 1350mW while keeping the Cold Tip temperature at 150K, considering in both cases, an interface temperature of 23ºC at the base. For a higher interface temperature of 71ºC, the thermal load is limited to 550mW and 1100mW, respectively. The heat flux at the mounting base of the cryocooler at these temperature ranges varies from 400 to 620 mW/cm^2 with an area of 21 cm^2 giving a load of 8.4 to 13 W for the mechanically pumped fluid loop.

As the cryocooler is mounted on the heat exchanger, its interface temperature at the base is driven by the capacity of the first stage of extracting the heat from the heat exchanger and rejecting it to the cold space. As it is discussed further, the heat exchanged by the fluid increases as fluid velocity increases, however, after some point, the heat generated from the pump overcomes the increase in the fluid heat exchange rate, and the heat exchanger temperature starts to rise again.

After a trade study on commercially available miniature pumps suitable for use within CubeSat, The pump selected and used in the first stage of the ACCS was the M510[5]. This pump has 100g of mass, and it can provide a flow rate of up to 9000ml/min with a power input of up to 28W. As anticipated in the design and further discussed in the system identification data analysis, the M510 is oversized for the ACCS project requirements and should operate in a lower power consumption mode.[3]

ACCS PHYSICAL MODELLING

A physical thermal model of the ACCS was developed using MATLAB SIMSCAPE. The diagram presented in Figure 4 shows the main blocks of the model. The yellow line connecting the blocks represents the thermal fluid connection that forms the closed-loop, where the NOVEC 7000[6] heat fluid circulates in the counterclockwise direction.

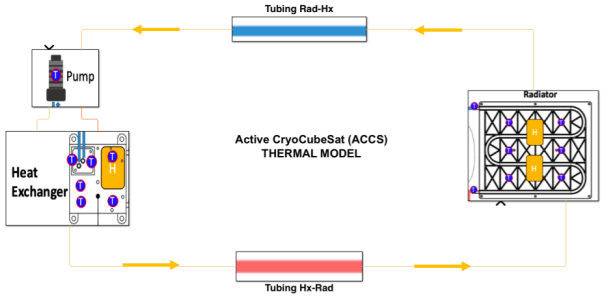

Figure 4: SIMSCAPE thermal model of the Active CryocubeSat (ACCS)

Pump block

The disconnected input port showing in the Pump block (Figure 4) corresponds to the Pump power input. Inside the Pump block, a user-defined function converts the pump power into a volumetric flow rate based on equation 1, which was derived fitting the measured data from the TVAC test, as shown in Figure 5.

$$\phi(P) = (a_1 e^{a_2 P} + a_3 e^{a_4 P}) * S\,[m^3/s] \quad (1)$$

$$a_1 = 0.3747,\ a_2 = 0.02342,$$

$$a_3 = -0.3742,\ a_4 = -0.4729,\ S = 29.5 * 10^{-6} m^2$$

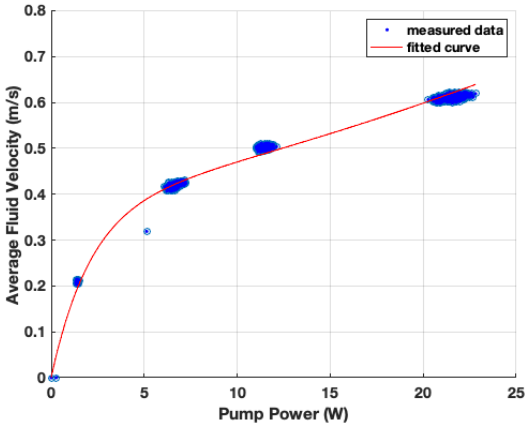

Figure 5: Data fitting for the pump characterization

As shown in Figure 4, between the Pump block and the Heat Exchanger block, in addition to the thermal fluid connection (yellow line), there is also a thermal connection (orange line), which thermally connects the blocks by conduction. Since the pump is physically mounted on top of the heat exchanger, part of the pump power is converted into heat and transferred by conduction to the heat exchanger.

Heat Exchanger block

Inside the heat exchanger block, see Figure 6, there is the definition of the HX thermal mass, where the HX mass and specific heat of its material are accounted for. The HX directly receives heat from the Pump, a secondary heater, and the Cryocooler.

The Cryocooler block has its own thermal mass and two internal heat sources: the cold tip thermal load and the heat generated by the Ricor motor. In essence, the cryocooler works as another MPFL stage in the system, with no thermal fluid interchange between both stages. It is self-controlled and it has the goal of maintaining the temperature at the cold tip stable at some cryogenic level. As presented later, during the TVAC test the Ricor power operated at around 8W to keep the cold tip temperature around 120K, with a cold tip thermal load at around 0.55W and with the heat exchanger temperature in the range of ± 5ºC. In this case, for example, from the heat exchanger model perspective, the Cryoocoler block is seen as a thermal load generating 8.55W of heat, which is transferred through their mechanical interface.

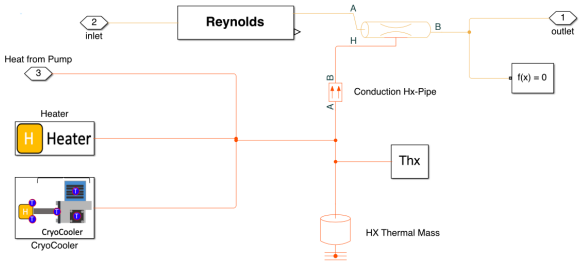

Figure 6: Heat Exchanger block

The Reynolds block shown in Figure 6 is used to monitor the Reynolds number of the fluid in the inlet of the HX during simulations.

The convection heat transfer for the internal flow inside the heat exchanger and the radiator is modeled considering that the fluid is fully developed along the entire tube, and the heat exchange coefficient follows from Nusselt number correlations.

The Nusselt number is considered to be 3.66 while in the laminar flow regime and computed from equation 1 in the turbulent flow regime. Equation 2 is the Gnielinski correlation, where f_{avg} is the Darcy friction factor at the average Reynolds number, Re_{avg}, and Pr_{avg} is the Prandtl number evaluated at the average temperature of the fluid.

$$Nu_{turb} = \frac{\frac{f_{avg}}{8}(Re_{avg} - 1000)Pr_{avg}}{1 + 12.7\sqrt{\frac{f_{avg}}{8}}(Pr_{avg}^{2/3} - 1)} \quad (2)$$

The model allows for the simulation of different ranges of Reynolds numbers for the transition between laminar and turbulent regimes. When the average Reynolds number is between the Laminar flow upper Reynolds number limit and the Turbulent flow lower Reynolds number limit, the model uses a Nusselt based smooth transition between the laminar and turbulent Nusselt number values.

Tubing blocks

Both intermediate tubbings connecting the heat exchanger outlet with the radiator inlet (red), and the radiator outlet with the pump inlet (blue) were modeled

as thermally isolated, therefore, no heat exchange by either conduction or radiation was considered between those tubings and their surroundings. Their thermal mass and their effect on pressure loss were taken into account in the model.

Radiator block

The radiator block shown in Figure 7 is similar to the heat exchanger block. Essentially, it has a thermal mass that exchanges heat by conduction with the tubing wall and radiates heat towards cold space. It has two direct heat sources: a heater and a block called Radiation from Sun and Earth.

The Radiation from the Sun and Earth block accounts for the energy received by the Sun and also the combined energy from the Earth's IR and albedo, based on the relative pointing direction.

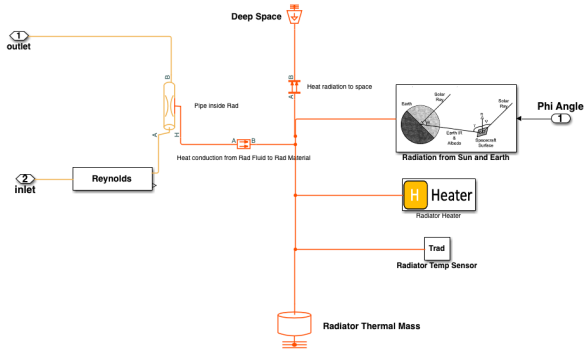

Figure 7: Radiator block

The ACCS radiator measures 0.3m x 0.2m. Its single-sided surface area of 0.06 m^2 is considered inside the Radiation from the Sun and Earth block to compute the effective area that receives incoming radiation. For perspective, considering all the parameters used in the block, the ACCS radiator may receive a maximum of 6.28W and a minimum of 0.52W, when its surface is perpendicular and parallel to solar rays, respectively during daylight. During eclipses, the ACCS radiator may still receive around 0.35W from Earth IR.

The rate of the heat transferred from the radiator to cold space is modeled using the Stefan-Boltzmann law. The emissivity considered was 92%. The total effective surface area considered was 0.161 m^2, which is approximately 34% larger than the doubled-sided geometric area of the radiator. This effective area was calculated using Monte Carlo simulation taking into account all the 3D physical aspects of the radiator surface. To simulate orbital flight, the cold space temperature is set to 7K, but to simulate the TVCA chamber environment, the cold space temperature was set to 95K. In practice, this difference in temperature is negligible in the computation of the heat rejection rate. For a radiator temperature at 300K, for example, the total rejected heat would be 68W for 7K cold space temperature and 67.3W for the TVAC chamber environment.

ACCS SYSTEM IDENTIFICATION

Data collection

As shown in Figure 8, for the data collection, the ACCS was instrumented with heaters mounted on the surface of the heat exchanger, cryocooler cold tip, and radiator to simulate different heat loads on the system. For temperature measurements, type T thermocouples were distributed across the different surfaces, and Lakeshore RTD DT 670 diodes were used to monitor the cryogenic temperature of the cryocooler's cold tip[7].

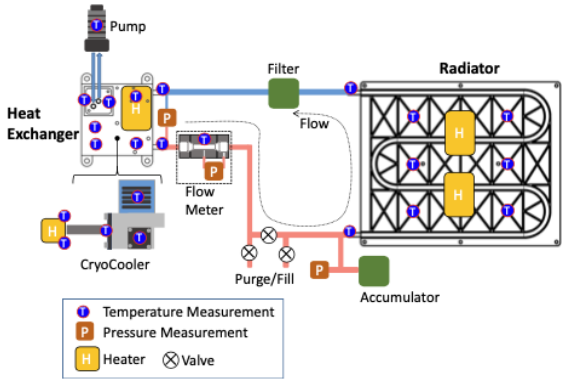

Figure 8: A system diagram of the Active CryoCubeSat mechanically pumped fluid loop testbed

The ACCS testbed was integrated with the data acquisition electronics and placed within the CSE/USU TVAC chamber.[6] The internal chamber pressure was kept under 10^{-5}mbar and the black-body rejection temperature under 95K.

The secondary heaters and pump power were set to the values presented in Table 1 and the system was allowed to reach thermodynamic equilibrium. Then a sequence of step inputs was performed to characterize the system. To determine the system response to perturbations around the baseline, the change in power followed the sequence: step down to a minimum level, step up to return to baseline, step up to maximum, and step down to return to baseline, see Figure 9. The baseline, minimum, and maximum power levels for each of the inputs are shown in Table 1. All power level transitions were conducted after a complete settle down of the system, and only one input was perturbed at a time.

Table 1: Baseline and range of the step inputs performed during TVAC test

Input	Baseline (W)	Min (W)	Max (W)
Pump power	6.6	1.4	21.5
Hx load	14.5	10.2	17.8
Rad load	9.85	4.8	15
CT load	0.55	0.28	0.80

Data was collected over 5.273610^5s (146:29:23, hh:mm:ss) in the thermal chamber, with a sample period of 9.2715 s/sample. The data analyzed and presented here is a cropped version of the collected data, starting at time 610^4s (16:40:00) and ending at time 3.3410^5s (92:46:40). Thus the total analyzed data time is 76:06:40.

Figure 9 shows the average temperature measured for both the heat exchanger surface and the cold tip during the step input sequence. The plot shows that the Cryocooler actively controlled the cold tip temperature during the test, keeping it stabled around 116K until 2 10^5s, when it experienced a drop to around 105K. After timestamp 216800s, the data also shows a temperature surge to around 120-130K that lasted for approximately 60 minutes, with a noticeable increase in the measurement noise. This temperature drop and oscillations likely occurred due to changes in grounding conducted during the test.

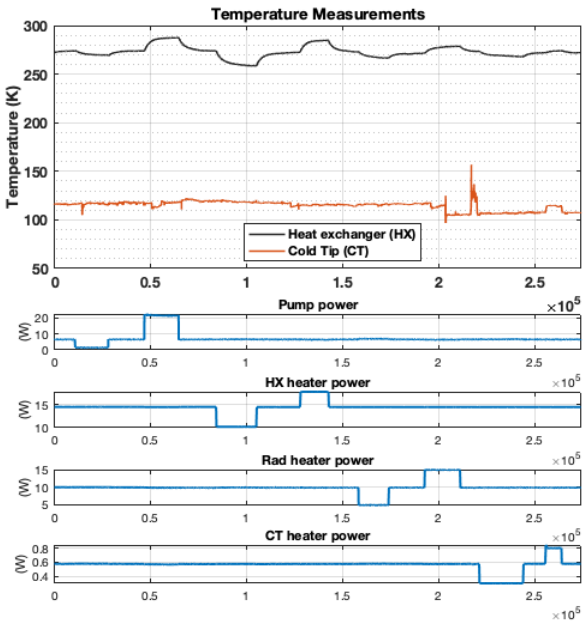

Figure 9: Temperature measurements of the heat exchanger surface and of the cold tip. Also showing the sequence of step inputs performed during the test.

Data analysis

The model identification presented here was performed using the MATLAB System Identification App. Before the system identification analysis was conducted, the test data was preprocessed to filter out the noise and remove offsets.

For the first analysis, a multiple-input single-output system was chosen to characterize the average temperature of the heat exchanger as a function of the pump power and all its heat sources. For this, four inputs were selected: pump power, heat exchanger heater's power, radiator heater's power, and Ricor motor's power. The average temperature of the heat exchanger was selected as the single output of the system. Figure 10 shows five temperature measurements taken at different locations of the heat exchanger that composes the average temperature of the heat exchanger.

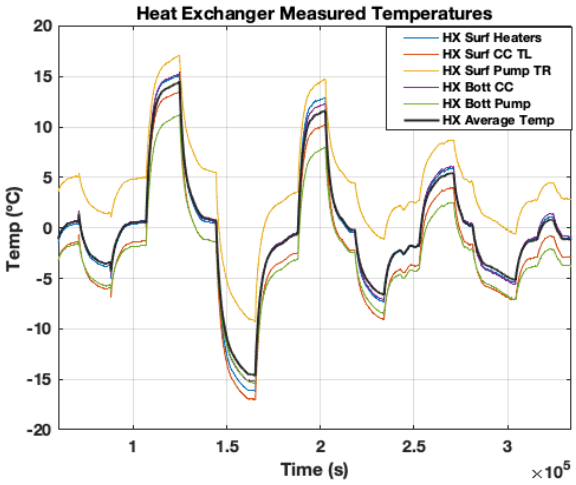

Figure 10: Measured temperatures on five different locations of the heat exchanger

Instead of using the cold tip power as one of the system inputs, the Ricor power was chosen in its replacement for having a more direct thermal connection with the heat exchanger. Besides that, the cryocooler controls the Ricor power to maintain the cold tip at the desired cryogenic temperature during the entire test, thus the heat generated from the Ricor operation constantly changes during the test, affecting the HX temperature.

For this system, different linear models with different orders were tested, and the best results in terms of fitting the measured data were found for low order models, see Figure 11. The simple linear model with one pole and no zeros for all four inputs had the best fit of 88.9%, and a model with two poles and one zero resulted in a slightly better fit of 89.7%.

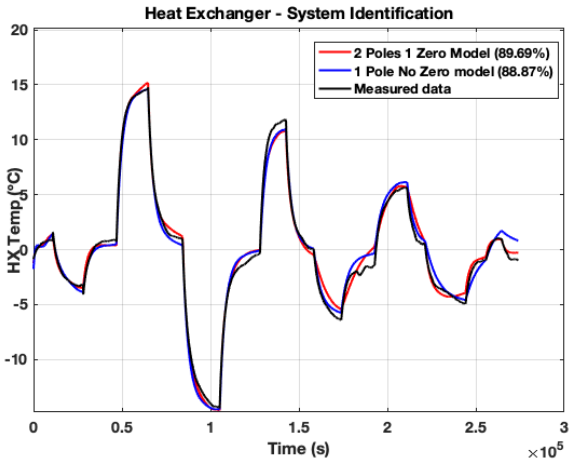

Figure 11: Heat exchanger model identification output plot

The parameters for the one pole no zero model of the Heat Exchanger temperature as a function of the pump power and other thermal loads are listed in Table 2.

Table 2: Parameters for the Heat Exchanger temperature one pole linear model (best-fit: 88.9%)

$Tf = a/(s+b)$	a	b
Pump power	299.8e-6	349.8e-6
HX Heater power	1095e-6	357.8e-6
Radiator power	316.2e-6	297.6e-6
Ricor pwr	201.2e-6	137e-6

The Cryocooler subsystem was also analyzed in terms of the Ricor power as a function of the Heat Exchanger temperature and the Cold Tip load. Similar to the heat exchanger, the best fitting results were found for low order models (see Figure 12). For the one pole no zero model, the best fit found was 82.2% and for two poles one zero model was 84.7%.

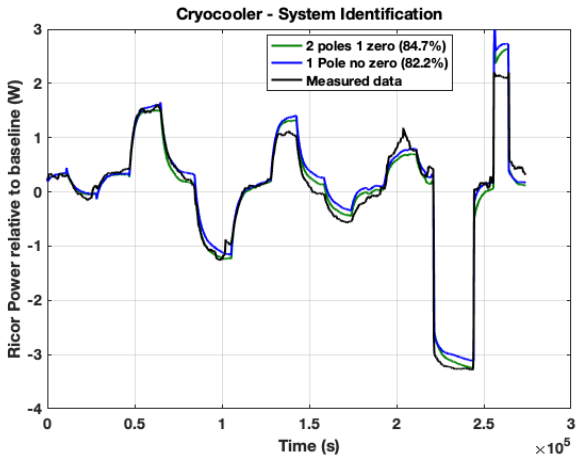

Figure 12: Cryocooler model identification output plot

Table 3 presents the parameters for the one pole no zero models of the Cryocooler power, represented by the Ricor power, as a function of the heat exchanger temperature and the cold tip thermal load power.

Table 3: Parameters for the Ricor power one pole linear model (best-fit: 82.2%)

$Tf = a/(s + b)$	a	b
HX Temperature	106.6e-3	1.093
CT load power	171.3e-3	16.39e-3

SIMULATIONS RESULTS

The physical model was validated against measured data and compared with the heat exchanger linear one pole no zero model prediction derived from the system identification. Figure 13 presents, on top, the average heat exchanger temperature predicted by both physical and linear models, plotted against the measured average temperature. All the models were subjected to the same power input signals measured during the TVAC chamber test, also shown in Figure 10.

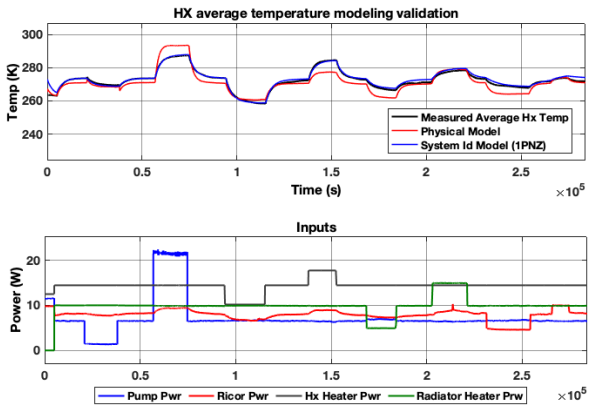

Figure 13: (top) comparison between the measured heat exchanger average temperature, the linear model prediction, and the physical model prediction. (bottom) all power inputs signals.

Even though the physical model presented a worse prediction of the measured data when compared to the linear model, it was capable of generating the same shape of all the input responses observed in the test, with slight offsets, less than 5K, in the equilibrium temperatures. We note that a more appropriate comparison between the models would be conducted using a completely independent dataset than the one used to generate the linear model in the system identification process, but this was not possible.

An important outcome of the physical modeling was the observation of the nonlinear behavior of the pump power with respect to the HX temperature. Intuitively, with an increment in the pump power and, consequently, in the fluid velocity, the capacity to transport heat from the HX to the radiator would increase, causing the temperature of the HX to decrease. The step responses of the average HX temperature to the power steps of the pump power presented between time 0s and 10^5s in Figure 13, however, suggest exactly the opposite behavior.

In fact, when the fluid is no longer in the laminar regime, the increase in flow rate results in higher Nusselt numbers and, therefore, the thermal fluid increases its capacity to exchange heat. On the other hand, as the flow rate increases, the friction between the fluid and the tubing walls increases rapidly, and the

pump has to compensate for the loss in pressure with a higher power.

Since the Nusselt number, in the turbulent regime, follows approximately a linear curve with the fluid velocity, considering small changes in the fluid property, see equation 1, and the pump power follows a parabolic curve with the fluid velocity, see Figure 5, above a certain level, the increment in fluid velocity requires more additional pump power than what is gained with the increase in fluid capacity to transport heat, consequently, the pump starts to act more like a heater on top of the heat exchanger.

To observe this aforementioned nonlinear behavior of the pump power, the ACCS physical model was simulated with the pump power going from 0W to 10W, while maintaining all other inputs at their respective baseline levels. The equilibrium average temperature of the HX predicted by the model is presented in Figure 14, considering different values of pump inefficiency. The pump inefficiency indicates in the model the percentage of the pump power that is ultimately converted to heat and transferred to the HX by conduction.

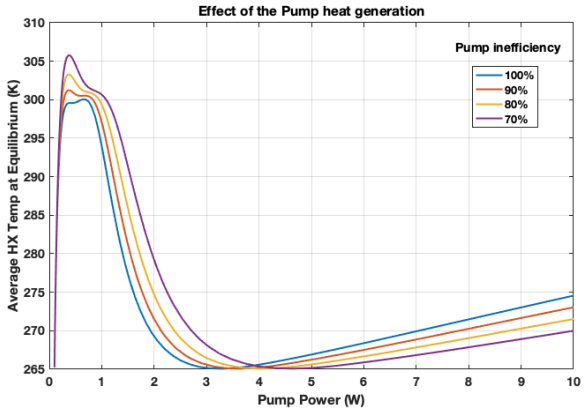

Figure 14: Effect of the pump heat generation as a function of its inefficiency on the curve of HX temperature as a function of the pump power. Transition regime Reynolds=[1000,4000]

The slope of the descent part of those curves and the minimum points are also affected by the Reynolds number of the start and end of the transition between laminar and turbulent. In this simulation, the start and end values were set to 1000 and 4000, respectively. The analysis of the collected data suggests that the end of the transition occurred at a much lower Reynolds number, around 2000.

The curves in Figure 14 show that for an interval of the pump power, in this case, from around 1W to 2W, the increment in pump power is overcome by an increase in the fluid convection heat transfer capability, and the temperature of HX decreases. For low pump power levels, less than approximately 250mW, the low convection heat coefficient of the laminar flow does not compensate for the heat generated by the pump, causing the HX temperature to increase. Finally, for higher than approximately 3W, as the pump power increases the temperature of the HX also increases proportionally.

The pump power behavior observed in the measured data, and linearized by the linear model through the system identification process, seems to be compatible with a high turbulent regime, where an increase in pump power causes an increase in the HX temperature. As it is discussed later, for a control designed perspective, where the goal is to keep the HX temperature at a certain level using the pump power as a control variable, the pump power shall be characterized and linearized in the descent portion of the curve, where the pump power has a negative gain towards the HX temperature.

CONTROL DESIGN

The TVAC test simulated the ACCS in a space environment where the cold tip temperature was kept in a pre-set cryogenic range of 100-120K by the Ricor cryocooler internal active control system, while the Heat exchanger temperature freely oscillated from -15ºC to 15ºC, as shown in Figure 9. For some space missions, however, this heat exchanger temperature oscillation might be undesirable. In such cases, a closed-loop feedback control system can be implemented to keep the HX temperature at a target value by adjusting the thermal fluid flow rate via the control of the pump's power.

Considering the same operation of the cryocooler conducted in the TVAC test and, as well as all other step inputs except the Pump's power, a conceptual PID

control was designed to control the Pump's power to maintain the average HX temperature at 288K.

As previously discussed, the linear model of the average HX temperature as a function of the Pump's power derived from the system identification process has shown not to be adequate to design an effective control of the HX temperature, since the linearization occurred in an operational range where an increment in pump power increases the HX temperature. For this reason, the PID control was tuned based on the nonlinear physical model and with the pump constrained to operate below 2.5W.

Table 4 presents the tuned Pump closed-loop PID parameters. Figure 15 shows the HX temperature control simulation using the Pump power as the actuator. As can be noticed, the HX temperature (red line) could be maintained close to the target value by the PID controller. The radiator temperature for the closed-loop controlled system is shown with the blue line. For comparison, the open-loop measured temperatures of the HX and radiator are also plotted with dashed lines.

Table 4: Parameters for the designed Pump PID control

$P + I/s + DN/(1 + N/s)$	
Proportional (P)	-0.102091175336817
Integral (I)	-0.00015118852314146
Derivative (D)	-6.77600075231049
Filter coefficient (N)	0.020742642213456

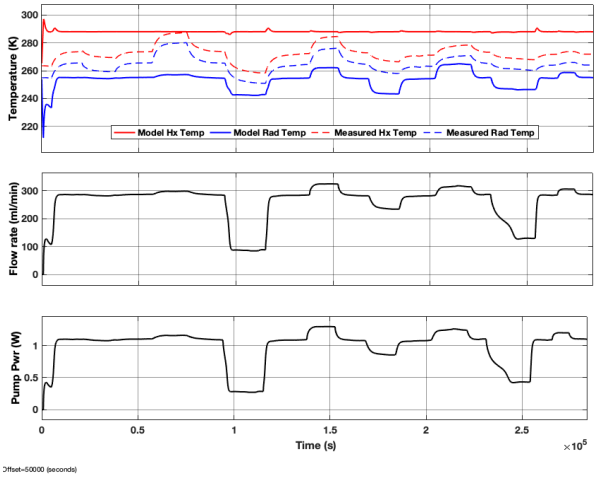

Figure 15: (top) controlled heat exchanger temperature, also showing radiator temperature and measured temperature from the open-loop TVAC test. (middle) thermal fluid flow rate. (bottom) controlled pump power.

Another set of simulations was run to determine the operational envelope of the controller for three different HX temperature setpoints. Table 5 presents the results. For each setpoint tested, the minimum HX thermal load was determined considering the case when sunlight is available and captured by the radiator surface, as well as when the ACCS is in eclipse or when the radiator is edge-on to the Sun. The maximum thermal load was determined considering no sunlight absorbed by the radiator and the pump operating close to its saturation at 2.5W.

Table 5: Minimum and maximum HX thermal loads for different HX temperature setpoints

	HX Thermal Load (W)		
HX temp setpoint (ºC)	Minimum (radiator collection sunlight)	Minimum (radiator not collecting sunlight)	Maximum (radiator not collecting sunlight)
0	2	5	35
15	3	7	44
30	4	14	54

These results show that for the use case of only a micro cryocooler as the Ricor K508N, which generates less than 12W of thermal load, mounted on top of the Heat exchanger, the ACCS would require additional heating in order to keep the HX thermal load over the minimum

value during eclipses, for the case of the HX temperature set to 30ºC. This suggests that the radiator surface area for ACCS was too large and must be tailored to the expected maximum thermal load and the desired setpoint of the HX temperature.

CONCLUSIONS

For the range of inputs performed during the TVAC test, the developed physical model showed to capture the main ACCS thermodynamic behavior and presented a close prediction for the heat exchanger average temperature. Additionally, the system identification conducted from the collected data provided a set of well-fitted low order linear models.

The analysis of the TVAC test data showed that the pump was tested in an excessive power range, where the effect of increasing the pump power to reduce the heat exchanger temperature was not observed. For this reason, even though the linear model derived from the system identification presented better performance explaining the measured data, the physical model was chosen to develop a conceptual heat exchanger temperature feedback closed-loop control system using the pump power as the control variable.

During simulations, the HX temperature control system presented satisfactory performance keeping the HX temperature stable around different setpoints. For a heat exchanger temperature set to 288K, the pump controller could handle thermal loads in the heat exchanger from 7 to 44W considering no sunlight captured by the radiator, with the pump consuming less than 2.5W.

The analysis results also suggested that the M510 pump has a significant excess of power when compared with what is needed to achieve the ACCS and ATA project thermal requirements, thus a smaller and less powerful pump might be selected for future optimized designs, if commercially available and suitable for the space applications.

Due to the nonlinearity nature of the pump operation during the transition between laminar and turbulent flow regimes, the simulation of the physical model for low pump power might not be accurate enough to design a robust thermal control system, therefore, another TVAC test with the pump operating in lower power range is necessary to validate the model.

Acknowledgments

The ATA team would like to thank the NASA SSTP office for their continued support and funding as well as the Jet Propulsions Laboratory for their encouragement and guidance.

In addition, the ACCS team would like to thank and acknowledge the wonderful student, faculty, and staff team at Utah State University. Without them, none of this would be possible.

Acronyms

- ACCS Active CryoCubeSat
- ATA Active Thermal Architecture
- CSE Center for Space Engineering
- HX Heat Exchanger
- IR Infrared
- JPL Jet Propulsion Laboratory
- MPFL Mechanically Pumped Fluid Loop
- NASA National Aeronautics and Space Administration
- SSTP Small Spacecraft Technology Program
- TVAC Thermal-Vacuum Chamber
- USU Utah State University

References

1. NASA, Active CryoCubeSat [Online] June 2017, https://ntrs.nasa.gov/archive/nasa/casi.ntrs.nasa.gov/201 60007914.pdf
2. Lucas S. Anderson, "Active Thermal Architecture: Design and Status" [Online] July 2020, https://digitalcommons.usu.edu/smallsat/2020/all2020/23/
3. Lucas S. Anderson, “The Active CryoCubeSat Project: Design and Status” [Online] June 2017, https://digitalcommons.usu.edu/smallsat/2017/all2017/1 54/

4. Integral Rotary Integral Stirling 1/2W Micro Cooler K508N [Online] June 2017, https://www.ricor.com/products/k508n/
5. M500 Series – Data Sheet [Online] June 2017, https://micropumps.co.uk/DATA/pdf/DS05%20-%20M500%20Data%20Sheet%20REV%206%20small.pdf
6. 3M™ Novec™ 7000 Engineered Fluid [Online] June 2017, http://multimedia.3m.com/mws/media/121372O/3m- novec-7000-engineered-fluid-tds.pdf
7. Lucas S. Anderson, "The Active CryoCubeSat Project: Testing and Preliminary Results" [Online] July 2018, https://digitalcommons.usu.edu/smallsat/2018/all2018/461/